

**Photovoltaic Hall effect in the two-dimensional electron gas: Kinetic theory**M. V. Durnev *Ioffe Institute, 194021 St. Petersburg, Russia*

(Received 9 June 2021; revised 30 July 2021; accepted 2 August 2021; published 17 August 2021)

We study theoretically transverse photoconductivity induced by circularly polarized radiation, i.e., the photovoltaic Hall effect, and linearly polarized radiation causing intraband optical transitions in the two-dimensional electron gas (2DEG). We develop a microscopic theory of these effects based on the analytical solution of the Boltzmann equation for arbitrary electron spectrum and scattering mechanisms. We calculate the transverse photoconductivity of 2DEG with parabolic and linear dispersion for short-range and Coulomb scatterers at different temperatures. We show that the transverse electric current is significantly enhanced at frequencies comparable to the inverse energy relaxation time, whereas at higher frequencies the excitation spectrum and the direction of current depend on the scattering mechanism. We also analyze the effect of thermalization processes caused by electron-electron collisions on the photoconductivity.

DOI: [10.1103/PhysRevB.104.085306](https://doi.org/10.1103/PhysRevB.104.085306)**I. INTRODUCTION**

Direct electric currents induced by high-frequency electric field in graphene and other two-dimensional (2D) materials have been the subject of active investigation in recent years [1,2]. In unbiased samples, the dc current is induced by oscillating electric and magnetic fields of the incident radiation through different mechanisms, including photothermoelectric [3–5], photovoltaic and bolometric [6], plasmonic [7–9], photon drag [10–12], bulk [13–19], and edge [20–22] photogalvanic effects. These mechanisms are relevant in 2D structures with broken space inversion symmetry due to crystal lattice,  $p$ - $n$  junctions, inhomogeneity of illumination, photon wave vectors, or edges. On the other hand, in a biased 2D layer, incident radiation may induce dc electric current, which flows in the direction perpendicular to the dc electric field, even if the system is spatially isotropic. For circularly polarized radiation, the appearance of such a transverse current is reminiscent of the Hall effect, and hence is termed the photovoltaic Hall effect [23].

The photoinduced anisotropy of conductivity was studied in early works in three-dimensional (3D) crystals and thin films [24–27]. It was shown that under illumination of a biased 3D crystal with circularly or linearly polarized electromagnetic waves, the transverse dc current appears, where direction is controlled by the radiation polarization. The interest in transverse photoconductivity has been recently renewed with an advent of graphene and 2D materials. The photovoltaic Hall effect and transverse photoconductivity induced by linearly polarized radiation in 2D layers are being actively studied both theoretically [23,28–32] and experimentally [33–35].

The anisotropic photoconductivity in 2D materials has been studied so far for high-frequency radiation, which induces interband optical transitions between the valence and conduction bands in the low-intensity regime [29–31], and

leads to the formation of dressed Floquet states in the high-intensity regime [23,30,32,36]. With decreasing the frequency of radiation, e.g., to the terahertz range, the interband transitions in doped structures become forbidden and intraband (Drude-like) optical transitions in the two-dimensional electron gas (2DEG) come into play. In that case, the Hall current is determined by the electron kinetics in the presence of ac and static electric fields and scattering impurities. Such a semiclassical kinetic description has been applied for Monte Carlo simulations of the transverse current in graphene [28], however, an analytical theory is still missing.

Here we study the photovoltaic Hall effect and transverse photoconductivity induced by linearly polarized radiation due to intraband optical transitions in the 2DEG. We develop a kinetic theory of anisotropic photoconductivity based on the analytical solution of the Boltzmann equation for an arbitrary momentum dependence of the electron energy and arbitrary scattering mechanism. The derived analytical expressions can be applied to calculate transverse photoconductivity in a large class of 2D materials with linear, parabolic, or Dirac energy dispersion, such as monolayer and bilayer graphene, monolayers of TMDC, and quantum wells. The developed theory also allows one to analyze in detail the influence of scattering mechanisms on the Hall current. We show that the Hall current contains two contributions: The first one is due to alignment of electron momenta by ac and static electric fields, and the second one is due to the dynamic heating and cooling of the 2DEG. The heating contribution is dominant in the frequency range  $\omega\tau_0 \lesssim 1$ , where  $\omega$  is the radiation frequency and  $\tau_0$  is the energy relaxation time. In this range, the transverse photoconductivity reaches  $\sim 1\%$  of the dark conductivity, i.e., conductivity in the absence of radiation, of 2DEG at  $1 \text{ W cm}^{-2}$  of the radiation intensity. At  $\omega\tau_0 \gg 1$ , the transverse photoconductivity is determined by the relaxation times of the first and second angular harmonics of the distribution function and their energy derivatives. In this case, the

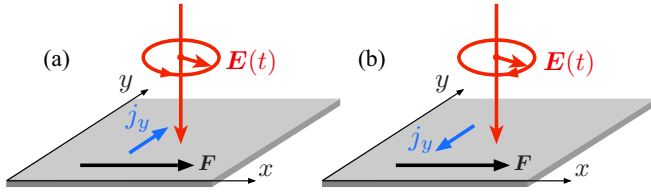


FIG. 1. The sketch of the photovoltaic Hall effect. Circularly polarized radiation induces transverse dc current, which direction is opposite for the right- (a) and left- (b) circular polarization.

excitation spectrum and even the sign of the transverse current are governed by the prevalent scattering mechanism. We also show that the thermalization process caused by electron-electron collisions has a low impact on the photoconductivity at low temperatures, however, may considerably alter the photoconductivity excitation spectrum with increasing temperature.

The paper is organized as follows. In Sec. II, we formulate the model and present kinetic equations. In Sec. III, we calculate transverse photoconductivity of 2DEG with parabolic energy dispersion. In Sec. IV, we calculate transverse photoconductivity of 2DEG with an arbitrary energy dispersion and apply the derived results to analyze the photoconductivity of graphene. In Sec. V, we study the role of the thermalization process on the photoconductivity, and in Sec. VI we summarize the results.

## II. MODEL AND KINETIC EQUATIONS

We consider the 2DEG in the  $(xy)$  plane subject to in-plane oscillating electric field  $\mathbf{E}(t) = \mathbf{E} \exp(-i\omega t) + \mathbf{E}^* \exp(i\omega t)$  and static electric field  $\mathbf{F}$ . In addition to the current along  $\mathbf{F}$ , the oscillating and static fields create the direct electric current, which flows in the direction perpendicular to  $\mathbf{F}$ . This transverse current appears for circularly and linearly polarized field  $\mathbf{E}(t)$  and changes direction when the polarization sign is changed, see Fig. 1.

In general, the photoinduced dc current in the isotropic 2DEG is determined by three constants  $\gamma_j$  [25]:

$$\mathbf{j} = \gamma_1 |\mathbf{E}|^2 \mathbf{F} + \gamma_2 [\mathbf{E}^* (\mathbf{E} \cdot \mathbf{F}) + \text{c.c.}] + i\gamma_3 [\mathbf{F} \times [\mathbf{E} \times \mathbf{E}^*]]. \quad (1)$$

Here,  $\gamma_1$  describes the change of isotropic conductivity under the action of radiation, whereas  $\gamma_2$  and  $\gamma_3$  describe the anisotropic photoconductivity induced by linearly and circularly polarized radiation, respectively. Below we calculate  $\gamma_2$  and  $\gamma_3$  due to intraband (Drude-like) optical transitions in the 2DEG. Note that Eq. (1) with no additional parameters also holds for the 2DEG in high-symmetry 2D crystals, such as graphene.

To calculate the transverse current, we introduce the electron distribution function in the momentum space  $f(\mathbf{p}, t)$ , which satisfies the Boltzmann equation:

$$\frac{\partial f}{\partial t} + e[\mathbf{F} + \mathbf{E}(t)] \cdot \frac{\partial f}{\partial \mathbf{p}} = \text{St } f. \quad (2)$$

Here  $\mathbf{p}$  is the electron momentum,  $e$  is the electron charge, the static electric field  $\mathbf{F}$  is parallel to the  $x$  axis, and  $\text{St } f$  is

the collision integral. Equation (2) is valid for the classical regime, when  $\hbar\omega \ll \bar{\epsilon}$ , where  $\bar{\epsilon}$  is the mean electron energy.

We solve Eq. (2) analytically by expanding the distribution function  $f(\mathbf{p}, t)$  in the series in the electric field amplitude as follows:

$$f(\mathbf{p}, t) = f_0 + \tilde{f}_1(\mathbf{p}) + [\tilde{f}_1(\mathbf{p})e^{-i\omega t} + \text{c.c.}] + \tilde{f}_2(\mathbf{p}) + [\tilde{f}_2(\mathbf{p})e^{-i\omega t} + \text{c.c.}] + \tilde{f}_3(\mathbf{p}). \quad (3)$$

In the absence of electric field, the electron distribution is equilibrium and described by the Fermi-Dirac function  $f_0$  with chemical potential  $\mu_0$  and temperature  $T_0$ . The first-order corrections  $\tilde{f}_1 \propto F$  and  $\tilde{f}_1 \propto E$  determine linear (Drude) conductivity, responsible for dc electric current and ac current oscillating at the field frequency, respectively. The second-order corrections  $\tilde{f}_2 \propto EE^*$  and  $\tilde{f}_2 \propto FE$ . The transverse dc current is determined by the third-order correction  $\tilde{f}_3 \propto FEE^*$ . Note that we do not consider second-order corrections  $\propto F^2$  and  $\propto E^2$ , since these corrections do not contribute to the Hall current. Considering the term  $e[\mathbf{F} + \mathbf{E}(t)] \cdot \partial f / \partial \mathbf{p}$  in Eq. (2) as a perturbation, we obtain the following equations for corrections to distribution function:

$$e\mathbf{F} \cdot \frac{\partial f_0}{\partial \mathbf{p}} = \text{St } \tilde{f}_1, \quad (4a)$$

$$-i\omega \tilde{f}_1 + e\mathbf{E} \cdot \frac{\partial f_0}{\partial \mathbf{p}} = \text{St } \tilde{f}_1, \quad (4b)$$

$$e\left(\mathbf{E}^* \cdot \frac{\partial \tilde{f}_1}{\partial \mathbf{p}} + \mathbf{E} \cdot \frac{\partial \tilde{f}_1^*}{\partial \mathbf{p}}\right) = \text{St } \tilde{f}_2, \quad (4c)$$

$$-i\omega \tilde{f}_2 + e\left(\mathbf{F} \cdot \frac{\partial \tilde{f}_1}{\partial \mathbf{p}} + \mathbf{E} \cdot \frac{\partial \tilde{f}_1}{\partial \mathbf{p}}\right) = \text{St } \tilde{f}_2, \quad (4d)$$

$$e\mathbf{F} \cdot \frac{\partial \tilde{f}_2}{\partial \mathbf{p}} + e\left(\mathbf{E}^* \cdot \frac{\partial \tilde{f}_2}{\partial \mathbf{p}} + \mathbf{E} \cdot \frac{\partial \tilde{f}_2^*}{\partial \mathbf{p}}\right) = \text{St } \tilde{f}_3. \quad (4e)$$

We use the relaxation time approximation for the collision integral. The relaxation of the first and second angular harmonics of the function  $f(\mathbf{p}, t)$  is described by the times  $\tau_1$  and  $\tau_2$  defined as  $\tau_1^{-1} = -\langle \mathbf{v} \text{St } f \rangle / \langle \mathbf{v} f \rangle$  and  $\tau_2^{-1} = -\langle v_x v_y \text{St } f \rangle / \langle v_x v_y f \rangle$ , respectively, where  $\mathbf{v} = \partial \epsilon / \partial \mathbf{p}$  is the electron velocity,  $\epsilon$  is energy, and the angular brackets denote averaging over  $\mathbf{p}$  directions. As shown below, the zeroth angular harmonic of  $f(\mathbf{p}, t)$  also contributes to the transverse current. To describe the relaxation of the zeroth angular harmonic  $\langle f(\mathbf{p}, t) \rangle$ , we use the following collision integral:

$$\text{St } \langle f \rangle = -\frac{\langle f \rangle - f_T(\mu, T)}{\tau_{ee}} - \frac{\langle f \rangle - f_0}{\tau_0}. \quad (5)$$

The first term on the right-hand side of Eq. (5) describes thermalization of the electron distribution toward the Dirac-Fermi distribution  $f_T$  caused by electron-electron collisions. The  $f_T$  distribution is characterized by chemical potential  $\mu$  and temperature  $T$  defined from the conservation of electron number and total energy  $\sum_{\mathbf{p}} f = \sum_{\mathbf{p}} f_T$  and  $\sum_{\mathbf{p}} \epsilon f = \sum_{\mathbf{p}} \epsilon f_T$ , where  $\epsilon$  is the electron energy. The thermalization is determined by the time  $\tau_{ee}$ . The second term on the right-hand side of Eq. (5) describes the energy relaxation by phonons determined by the time  $\tau_0$ . In what follows, we consider  $\tau_{ee}$  and  $\tau_0$  independent of energy, but, generally,  $\tau_0$  and  $\tau_{ee}$  depend on temperature. Further, we consider a temperature

range where  $\tau_{1,2} \ll \tau_{ee} \ll \tau_0$ . This inequality is relevant for the 2DEG at low temperatures, however, may also hold at higher temperatures if the phonon-assisted energy relaxation is suppressed, as in the case of graphene [37,38].

The transverse current is determined by  $\tilde{f}_3$  and given by

$$j_y = eg \sum_p v_y \tilde{f}_3, \quad (6)$$

where  $g$  is the factor of spin and valley degeneracy. Multiplying Eq. (4e) by  $v_y$  and averaging the result over the directions of  $\mathbf{p}$ , we obtain

$$\langle v_y \tilde{f}_3 \rangle = -e\tau_1 \left\langle v_y \left( \mathbf{F} \cdot \frac{\partial \tilde{f}_2}{\partial \mathbf{p}} + \mathbf{E}^* \cdot \frac{\partial \tilde{f}_2}{\partial \mathbf{p}} + \mathbf{E} \cdot \frac{\partial \tilde{f}_2^*}{\partial \mathbf{p}} \right) \right\rangle. \quad (7)$$

Summation of Eq. (7) over  $\mathbf{p}$  and integration by parts yield

$$j_y = e^2 g \sum_p (\tilde{f}_2 \mathbf{F} + \tilde{f}_2 \mathbf{E}^* + \tilde{f}_2^* \mathbf{E}) \cdot \frac{\partial (v_y \tau_1)}{\partial \mathbf{p}}. \quad (8)$$

Equation (8) is used further to calculate transverse current for the 2DEG with arbitrary dispersion  $\varepsilon(|\mathbf{p}|)$ .

### III. ELECTRON GAS WITH PARABOLIC DISPERSION

We start with calculating  $j_y$  for parabolic energy dispersion of electrons  $\varepsilon(p) = p^2/2m$ , where  $m$  is the effective mass, and  $p = |\mathbf{p}|$ . This important limit also helps to clarify the basic physics of the effect. Calculating derivative on the right-hand side of Eq. (8), one obtains

$$j_y = e^2 g F \sum_p v_x v_y \tau_1' \tilde{f}_2 + \frac{e^2 g}{m} \sum_p (\tau_1 \varepsilon)' (E_y^* \tilde{f}_2 + E_y \tilde{f}_2^*) + \frac{e^2 g}{2} \sum_p [2v_x v_y E_x^* \tilde{f}_2 - (v_x^2 - v_y^2) E_y^* \tilde{f}_2 + \text{c.c.}] \tau_1'. \quad (9)$$

Here  $(\dots)' = \partial(\dots)/\partial \varepsilon$ , and we took into account that  $\mathbf{F} \parallel \mathbf{x}$ . Electric current Eq. (9) contains three contributions. The first one, proportional to  $v_x v_y \tilde{f}_2$ , is related to the optical alignment of electron momenta by the oscillating electric field [39–43]. Optical alignment results in excess electrons and holes below the Fermi level with velocities directed at  $\pi/4$  and  $3\pi/4$  with respect to the  $x$  axis. Together with the static electric field, which causes imbalance between charge carriers with  $v_x > 0$  and  $v_x < 0$ , it results in a net  $y$  current. The second term in Eq. (9), proportional to  $(\tau_1 \varepsilon)' \tilde{f}_2$ , is related to the dynamic heating and cooling of 2DEG by the combined action of static and oscillating fields [24]. Electrons periodically gain and lose their energy with a rate proportional to  $(\mathbf{F} \cdot \mathbf{E})$  and oscillating in time at frequency  $\omega$ . In turn, the  $E_y^*$  component of the incident field drives the electrons along the  $y$  direction. At the first and second half-periods of an oscillation cycle, both distribution of velocities and momentum relaxation times of electrons are different, which results in a net electric current. Finally, the third contribution to electric current Eq. (9) is related to dynamic optical alignment of charge carrier momenta by combined action of  $\mathbf{E}(t)$  and  $\mathbf{F}$ . The first and second contributions in Eq. (9) yield transverse photoconductivity for linearly polarized radiation with nonzero  $E_x E_y^* + E_x^* E_y$ ,

whereas the second and third contributions result in the photovoltaic Hall effect.

Solutions of Eqs. (4a) and (4b) for the first-order corrections to the distribution function are

$$\tilde{f}_1 = -e\tau_1 (\mathbf{F} \cdot \mathbf{v}) f_0', \quad \tilde{f}_1 = -e\tau_{1\omega} (\mathbf{E} \cdot \mathbf{v}) f_0', \quad (10)$$

where  $\tau_{1\omega} = \tau_1/(1 - i\omega\tau_1)$ . Substituting Eq. (10) in Eqs. (4c) and (4d) and solving the kinetic equations, we obtain for the second-order corrections

$$\begin{aligned} \tilde{f}_2 &= \langle \tilde{f}_2 \rangle + e^2 |\mathbf{E}|^2 \tau_2 (\text{Re}\{\tau_{1\omega}\} f_0') [S_1 (v_x^2 - v_y^2) + 2S_2 v_x v_y], \\ \tilde{f}_2 &= \langle \tilde{f}_2 \rangle + \frac{e^2 F \tau_{2\omega} [(\tau_{1\omega} + \tau_1) f_0']}{2} \\ &\quad \times [E_x (v_x^2 - v_y^2) + 2E_y v_x v_y], \end{aligned} \quad (11)$$

where  $S_1 = (|E_x|^2 - |E_y|^2)/|\mathbf{E}|^2$  and  $S_2 = (E_x E_y^* + E_x^* E_y)/|\mathbf{E}|^2$  are the Stokes parameters of the radiation polarization,  $\tau_{2\omega} = \tau_2/(1 - i\omega\tau_2)$ , and  $\text{Re}$  stands for real part. As seen from Eqs. (11), the functions  $\tilde{f}_2$  and  $\tilde{f}_2^*$  are sums of the zeroth and second angular harmonics in momentum space. Further in this section, we neglect thermalization by setting  $\tau_{ee} \rightarrow \infty$  in Eq. (5), and hence find  $\langle \tilde{f}_2 \rangle = -e\tau_{0\omega} (\mathbf{F} \cdot \partial \tilde{f}_1 / \partial \mathbf{p} + \mathbf{E} \cdot \partial \tilde{f}_1 / \partial \mathbf{p})$  from Eq. (4d). As shown in Sec. V, the neglect of thermalization is eligible at low temperatures of the 2DEG.

Substitution of Eqs. (11) in Eq. (9) for the current, averaging over  $\mathbf{p}$  directions and integration by parts yield

$$\begin{aligned} j_y &= -\frac{e^4 g F |\mathbf{E}|^2}{m^2} \\ &\quad \times \left\{ S_2 \text{Re} \sum_p [(\varepsilon^2 \tau_1' \tau_2)' \tau_{1\omega} + \varepsilon (\tau_1 \varepsilon)'' \tau_{0\omega} (\tau_{1\omega} + \tau_1)] f_0' \right. \\ &\quad \left. - S_3 \text{Im} \sum_p [(\varepsilon^2 \tau_1' \tau_{2\omega})' - \varepsilon (\tau_1 \varepsilon)'' \tau_{0\omega}] (\tau_{1\omega} + \tau_1) f_0' \right\}, \end{aligned} \quad (12)$$

where  $\tau_{0\omega} = \tau_0/(1 - i\omega\tau_0)$ , and  $S_3 = i(E_x E_y^* - E_x^* E_y)/|\mathbf{E}|^2$  is the degree of circular polarization. Finally, Eqs. (1) and (12) yield at  $T_0 = 0$ :

$$\begin{aligned} \gamma_2 &= \frac{\sigma_0 e^2}{m} \text{Re}\{(\varepsilon_F \tau_1'' + 2\tau_1') \alpha_\omega \tau_{0\omega} \\ &\quad + (1 - i\omega\tau_1)^{-1} [2\tau_1' \tau_2 + \varepsilon_F (\tau_1' \tau_2)']\}, \\ \gamma_3 &= \frac{\sigma_0 e^2}{m} \text{Im}\{(\varepsilon_F \tau_1'' + 2\tau_1') \alpha_\omega \tau_{0\omega} \\ &\quad - \alpha_\omega [2\tau_1' \tau_{2\omega} + \varepsilon_F (\tau_1' \tau_{2\omega})']\}, \end{aligned} \quad (13)$$

where  $\alpha_\omega = (2 - i\omega\tau_1)/(1 - i\omega\tau_1)$ ,  $\sigma_0 = e^2 n \tau_1 / m$  is the dark conductivity of the 2DEG,  $n = g m \varepsilon_F / (2\pi \hbar^2)$  is the electron density, and all energy-dependent quantities are taken at the Fermi energy  $\varepsilon_F$ . Equations (13) can be applied to different scattering mechanisms of 2D electrons characterized by the energy dependence of  $\tau_1$  and  $\tau_2$ . Particularly, it is seen that short-range scattering yielding  $\tau_1$  and  $\tau_2$  independent of energy does not contribute to the transverse photoconductivity of 2DEG with parabolic spectrum.

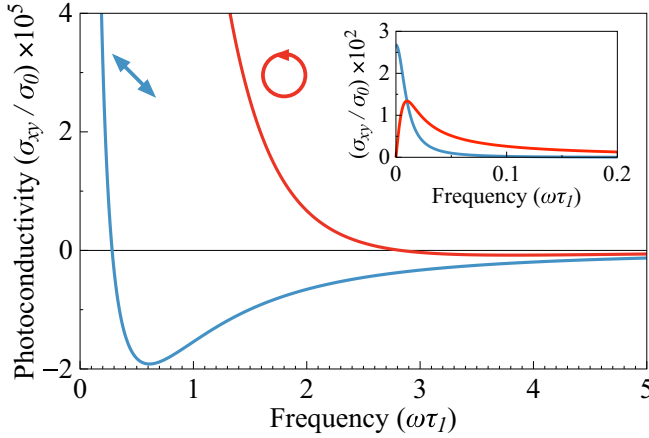


FIG. 2. Transverse photoconductivity of 2DEG with parabolic spectrum induced by linearly (blue lines) and circularly (red lines) polarized radiation. The inset shows the behavior at low frequencies  $\omega\tau_0 \lesssim 1$ . The curves are calculated after Eqs. (13) with  $\tau_1 = 2\tau_2 \propto \varepsilon$  corresponding to Coulomb scatterers.  $I = 1 \text{ W/cm}^2$ ,  $\tau_1 = 1 \text{ ps}$ ,  $\tau_0 = 100\tau_1$ ,  $m = 0.03 m_0$ ,  $\varepsilon_F = 50 \text{ meV}$ ,  $n_\omega = 3$ .

Figure 2 shows the photoconductivity induced by linearly polarized radiation,  $\sigma_{xy} = \gamma_2 |\mathbf{E}|^2$ , and by circularly polarized radiation,  $\sigma_{xy} = \gamma_3 |\mathbf{E}|^2$ . Coefficients  $\gamma_{2,3}$  are calculated after Eqs. (13) with  $\tau_1 = 2\tau_2 \propto \varepsilon$  corresponding to unscreened Coulomb scatterers. The parameters used for calculations are given in the caption of Fig. 2 and correspond approximately to bilayer graphene [21]. The curves are calculated for  $I = 1 \text{ W/cm}^2$ , where  $I = cn_\omega |\mathbf{E}|^2 / 2\pi$  is the intensity of radiation, and  $n_\omega$  is the refraction index of the medium surrounding the 2DEG. At  $\omega\tau_0 \lesssim 1$ , the photoconductivity is dominated by the first contribution in Eqs. (13) related to the heating mechanism. This contribution is on the order of  $\sigma_0 \xi$ , where  $\xi = e^2 |\mathbf{E}|^2 \tau_1 \tau_0 / (m \varepsilon_F)$  is the dimensionless parameter. Its value is  $\xi \approx 7 \times 10^{-3}$  for used parameters. The heating contribution decays at first within the narrow frequency range  $\omega\tau_0 \sim 1$ . At  $\omega\tau_0 \gg 1$ , the heating contribution and the second contribution in Eqs. (13) related to optical alignment are comparable. They both decay within a much wider frequency range  $\omega\tau_1 \sim 1$ , and the photoconductivity is determined by the interplay of both. In this frequency range,  $\sigma_{xy}/\sigma_0 \sim \xi \tau_1/\tau_0 \approx 7 \times 10^{-5}$ . Interestingly, interplay of two contributions may result in the change of transverse current sign with increasing frequency, as illustrated in Fig. 2. Similar to the Drude conductivity, at  $\omega\tau_1 \gg 1$  the anisotropic photoconductivity tends to zero. In that case, the rapidly oscillating field cannot deflect electrons toward the  $y$  direction.

#### IV. ELECTRON GAS WITH AN ARBITRARY DISPERSION

Let us now calculate transverse photoconductivity for an arbitrary energy dispersion of electrons  $\varepsilon(\mathbf{p})$ . We introduce an energy-dependent effective electron mass  $m(\varepsilon) = p/v$ , where  $p = |\mathbf{p}|$  and  $v = \partial \varepsilon / \partial p$ . We start with the general Eq. (8) for the current. After calculating the derivatives on the

right-hand side of Eq. (8), one obtains

$$j_y = e^2 g F \sum_{\mathbf{p}} v_x v_y m \left( \frac{\tau_1}{m} \right)' \tilde{f}_2 + e^2 g \sum_{\mathbf{p}} \left[ \frac{\tau_1}{m} + \frac{mv^2}{2} \left( \frac{\tau_1}{m} \right)' \right] (E_y^* \tilde{f}_2 + E_y \tilde{f}_2^*) + \frac{e^2 g}{2} \sum_{\mathbf{p}} [2v_x v_y E_x^* \tilde{f}_2 - (v_x^2 - v_y^2) E_y^* \tilde{f}_2 + \text{c.c.}] m \left( \frac{\tau_1}{m} \right)' \quad (14)$$

To calculate the first contribution on the right-hand side of Eq. (14), one should multiply Eq. (4c) for the distribution function  $\tilde{f}_2$  by  $v_x v_y m (\tau_1/m)'$  and sum the result over  $\mathbf{p}$ . The remaining two contributions are calculated in the same way using Eq. (4d). Integration by parts in the derived expressions yields

$$j_y = e^3 g F \sum_{\mathbf{p}} \tilde{f}_1 \mathbf{E}^* \cdot \frac{\partial}{\partial \mathbf{p}} \left[ \tau_2 v_x v_y m \left( \frac{\tau_1}{m} \right)' \right] + e^3 g \tau_{0\omega} \sum_{\mathbf{p}} E_y^* (\tilde{f}_1 \mathbf{F} + \tilde{f}_1 \mathbf{E}) \cdot \frac{\partial}{\partial \mathbf{p}} \left[ \frac{\tau_1}{m} + \frac{mv^2}{2} \left( \frac{\tau_1}{m} \right)' \right] + \frac{e^3 g}{2} \sum_{\mathbf{p}} (\tilde{f}_1 \mathbf{F} + \tilde{f}_1 \mathbf{E}) \cdot \frac{\partial}{\partial \mathbf{p}} \left[ \tau_{2\omega} m \left( \frac{\tau_1}{m} \right)' [2E_x^* v_x v_y - E_y^* (v_x^2 - v_y^2)] \right] + \text{c.c.} \quad (15)$$

Finally, substitution of Eqs. (10) for  $\tilde{f}_1$  and  $\tilde{f}_1$  in Eq. (15), calculation of derivatives on the right-hand side of Eq. (15) and summation over  $\mathbf{p}$  at  $T_0 = 0$  yields

$$\gamma_2 = \sigma_0 e^2 \text{Re} \left\{ \alpha_\omega \tau_{0\omega} \left[ \frac{\tau_1}{m} + \frac{mv^2}{2} \left( \frac{\tau_1}{m} \right)' \right] + \frac{m^2 v^2}{2(1 - i\omega\tau_1)} \left[ \frac{\tau_2}{m} \left( \frac{\tau_1}{m} \right)' \right]' + \frac{2\tau_2}{1 - i\omega\tau_1} \left( \frac{\tau_1}{m} \right)' \right\},$$

$$\gamma_3 = \sigma_0 e^2 \text{Im} \left\{ \alpha_\omega \tau_{0\omega} \left[ \frac{\tau_1}{m} + \frac{mv^2}{2} \left( \frac{\tau_1}{m} \right)' \right] - \frac{\alpha_\omega m^2 v^2}{2} \left[ \frac{\tau_{2\omega}}{m} \left( \frac{\tau_1}{m} \right)' \right]' - 2\alpha_\omega \tau_{2\omega} \left( \frac{\tau_1}{m} \right)' \right\}, \quad (16)$$

where  $\sigma_0 = e^2 n \tau_1 / m$  is the dark conductivity of the 2DEG and energy-dependent quantities are taken at  $\varepsilon_F$ .

Equations (16) are general and can be used to calculate anisotropic photoconductivity of the 2DEG with arbitrary energy dispersion  $\varepsilon(p)$  and for arbitrary energy dependence of relaxation times. For parabolic dispersion,  $m$  is energy independent,  $mv^2/2 = \varepsilon$ , and Eqs. (16) are reduced to Eqs. (13) obtained in Sec. III. For linear dispersion  $\varepsilon = v_0 p$ , relevant to graphene, one has  $m = \varepsilon/v_0^2$  and  $mv^2 = \varepsilon$ . Let us calculate  $\gamma_2^{(\delta)}$  and  $\gamma_3^{(\delta)}$  for short-range (deltalike) scatterers in graphene.



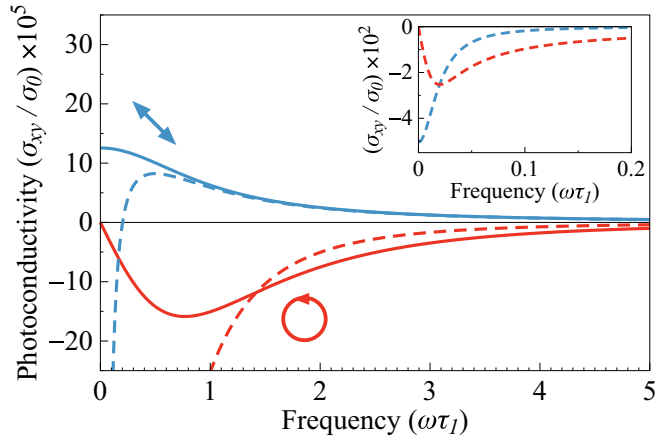


FIG. 3. Transverse photoconductivity of 2DEG in graphene induced by linearly (blue lines) and circularly (red lines) polarized radiation. The inset shows the behavior at low frequencies  $\omega\tau_0 \lesssim 1$ . The solid curves are calculated after Eqs. (17) with  $\tau_1 = 2\tau_2 \propto \varepsilon^{-1}$  corresponding to short-range scatterers. The dashed curves are calculated after Eqs. (16) with  $\tau_1 = 2\tau_2 \propto \varepsilon/(\varepsilon^2 + \varepsilon_0^2)$  corresponding to a mixture of Coulomb and short-range scatterers.  $I = 1 \text{ W/cm}^2$ ,  $\tau_1 = 1 \text{ ps}$ ,  $\tau_0 = 100\tau_1$ ,  $\varepsilon_F = \varepsilon_0 = 50 \text{ meV}$ ,  $v_0 = 10^8 \text{ cm/s}$ ,  $n_\omega = 3$ .

In that case,  $\tau_1 = 2\tau_2 \propto \varepsilon^{-1}$  and Eqs. (16) yield

$$\gamma_2^{(\delta)} = \frac{\sigma_0 e^2 v_0^2 \tau_1^2}{2\varepsilon_F^2 (1 + \omega^2 \tau_1^2)}, \quad \gamma_3^{(\delta)} = -\frac{12\omega\tau_1}{4 + \omega^2 \tau_1^2} \gamma_2. \quad (17)$$

Figure 3 shows the photoconductivity induced by linearly polarized radiation,  $\sigma_{xy} = \gamma_2 |\mathbf{E}|^2$ , and by circularly polarized radiation,  $\sigma_{xy} = \gamma_3 |\mathbf{E}|^2$  in graphene. Coefficients  $\gamma_{2,3}$  are calculated after Eqs. (17) for short-range scatterers and after Eqs. (16) with  $\tau_1 = 2\tau_2 \propto \varepsilon/(\varepsilon^2 + \varepsilon_0^2)$  corresponding to mixture of Coulomb and short-range scatterers;  $\varepsilon_0$  is a parameter. Note that the heating contribution vanishes in graphene with short-range scatterers, and hence the photoconductivity Eqs. (17) are independent of  $\tau_0$ . However, the addition of Coulomb centers restores the heating contribution and significantly enhances the photoconductivity at  $\omega\tau_0 \lesssim 1$ . Note that scattering solely at the Coulomb centers yields  $\tau_{1,2} \propto \varepsilon$  resulting in  $\sigma_{xy} = 0$ . The values of  $\sigma_{xy}/\sigma_0$  at  $\omega\tau_0 \gg 1$  are about an order of magnitude larger in monolayer graphene than in bilayer graphene, see Fig. 2, due to the smaller effective mass of electrons in graphene.

## V. ROLE OF FINITE TEMPERATURE AND THERMALIZATION

In this section, we calculate the transverse photoconductivity of 2DEG at finite temperature. At finite temperature, the distribution function of 2DEG is smeared over energy and thermalization processes caused by electron-electron collisions affecting the kinetics of the zeroth angular harmonic  $\langle f \rangle$  of the distribution function. We describe this kinetics by the collision integral Eq. (5). We assume that in the absence of external fields  $\mathbf{F} = 0$ ,  $\mathbf{E} = 0$ , the temperature of the 2DEG is  $T_0$  and its chemical potential  $\mu_0$ . Heating or cooling of the gas by combined action of incident radiation and static electric field and fast electron-electron collisions result in a

different temperature  $T$  and chemical potential  $\mu$  of the electron subsystem. Further, we discuss the thermalization of the oscillating correction  $\tilde{f}_2 \exp(-i\omega t) + \text{c.c.}$  to the distribution function of 2D electrons, since this correction determines the heating contribution to the current in Eq. (14). Therefore,  $T$  and  $\mu$  also oscillate with frequency  $\omega$ .

To determine  $T$ , one should calculate the change of the total electron energy  $\Delta E(t)$  at a given moment of time and consider how it is redistributed between thermalized electrons. The change of the total electron energy is

$$\Delta E = \sum_p \varepsilon(f - f_0) = \sum_p \varepsilon[f_T(\mu, T) - f_0], \quad (18)$$

because  $\sum_p \varepsilon f = \sum_p \varepsilon f_T(\mu, T)$ . Assuming  $\Delta T/T_0 \ll 1$ , where  $\Delta T = T - T_0$ , one has

$$\Delta E \approx \frac{\Delta T \sum_p \varepsilon A}{T_0}, \quad (19)$$

where

$$A(\varepsilon) = -\left[ \varepsilon - \mu_0 + T_0 \frac{d\mu}{dT}(T_0) \right] f'_0, \quad (20)$$

and  $d\mu/dT$  can be found from the particle conservation constraint  $\sum_p [f_T(\mu, T) - f_0] = 0$ . On the other hand,  $\Delta E$  is found from Eq. (4d), bearing in mind that thermalization conserves the total energy of the 2DEG. Taking into account Eq. (19), one thus finds

$$\frac{\Delta T}{T_0} = \frac{\tau_{0\omega} \sum_p G\varepsilon}{\sum_p \varepsilon A} e^{-i\omega t} + \text{c.c.}, \quad (21)$$

where

$$G = -e \left\langle \mathbf{F} \cdot \frac{\partial \tilde{f}_1}{\partial \mathbf{p}} + \mathbf{E} \cdot \frac{\partial \tilde{f}_1}{\partial \mathbf{p}} \right\rangle. \quad (22)$$

Solution of the kinetic Eq. (4d) with the collision integral Eq. (5) and  $\Delta T$  given by Eq. (21) yields

$$\langle \tilde{f}_2 \rangle = \frac{\tau_{0\omega}}{\tau_{0\omega} + \tau_{ee}} \left( G\tau_{ee} + A \frac{\tau_{0\omega} \sum_p G\varepsilon}{\sum_p A\varepsilon} \right). \quad (23)$$

Equation (23) is then used to calculate the heating contribution to the electric current in Eq. (14). Computation analogous to the one in Sec. IV yields

$$\begin{aligned} \gamma_2 &= \sigma_0 e^2 \text{Re} \left\langle \alpha_\omega \tau_{0\omega} H + \frac{2\tau_2}{1 - i\omega\tau_1} \left( \frac{\tau_1}{m} \right)' \right. \\ &\quad \left. + \frac{m^2 v^2}{2(1 - i\omega\tau_1)} \left[ \frac{\tau_2}{m} \left( \frac{\tau_1}{m} \right)' \right] \right\rangle_\varepsilon, \\ \gamma_3 &= \sigma_0 e^2 \text{Im} \left\langle \alpha_\omega \tau_{0\omega} H - 2\alpha_\omega \tau_{2\omega} \left( \frac{\tau_1}{m} \right)' \right. \\ &\quad \left. - \frac{\alpha_\omega m^2 v^2}{2} \left[ \frac{\tau_{2\omega}}{m} \left( \frac{\tau_1}{m} \right)' \right] \right\rangle_\varepsilon. \end{aligned} \quad (24)$$

Here  $H$  is given by

$$H = \frac{\tau_{ee}}{\tau_{0\omega} + \tau_{ee}} Q' + \frac{\tau_{0\omega}}{\tau_{0\omega} + \tau_{ee}} \frac{\sum_p A Q}{\sum_p A \varepsilon}, \quad (25)$$

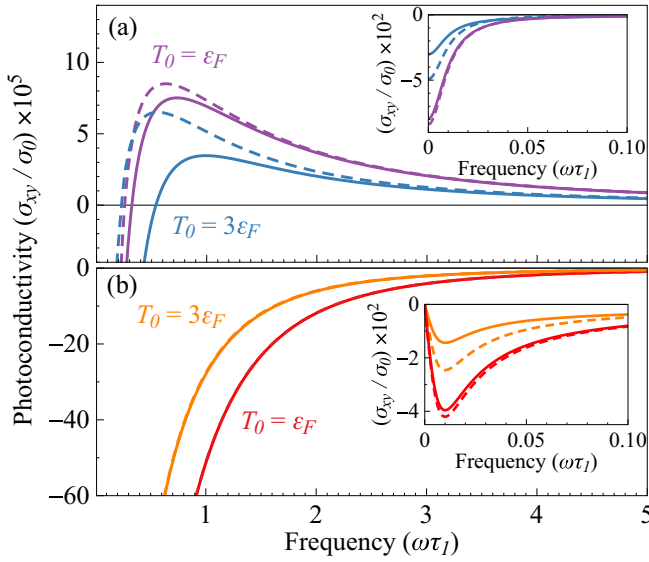


FIG. 4. Transverse photoconductivity of 2DEG in graphene at nonzero temperature for linearly (a) and circularly (b) polarized radiation. The inset shows the behavior at low frequencies  $\omega\tau_0 \lesssim 1$ . The curves are calculated after Eqs. (24) with  $\tau_{ee} = 10\tau_1$  (solid) and  $\tau_{ee} = +\infty$  (dashed).  $\tau_1 = 2\tau_2 \propto \varepsilon/(\varepsilon^2 + \varepsilon_0^2)$ ,  $\varepsilon_0 = 50$  meV,  $\varepsilon_F = 10$  meV,  $I = 1$  W/cm<sup>2</sup>,  $\tau_1(\varepsilon_0) = 1$  ps,  $\tau_0 = 100\tau_1$ ,  $v_0 = 10^8$  cm/s,  $n_\omega = 3$ .

with

$$Q = \frac{\tau_1}{m} + \frac{mv^2}{2} \left( \frac{\tau_1}{m} \right)', \quad (26)$$

and the energy averaging  $\langle \dots \rangle_\varepsilon$  is defined as

$$\langle \dots \rangle_\varepsilon = \frac{\sum_p (\dots) v^2 \tau_1 f'_0}{\sum_p v^2 \tau_1 f'_0}. \quad (27)$$

Equation (24) allows one to calculate the transverse photoconductivity of the 2DEG at a given temperature  $T_0$ . At  $T_0 = 0$ , one has  $\sum_p A Q / \sum_p A \varepsilon = Q'(\mu_0)$  and, as follows from Eq. (25),  $H(\mu_0) = Q'(\mu_0)$ . In that case, thermalization does not affect the photoconductivity, and  $\gamma_{2,3}$  coincide with those given by Eq. (16). Figure 4 presents the transverse photoconductivity  $\sigma_{xy} = \gamma_{2,3} |E|^2$  calculated after Eq. (24) for graphene. Calculations are done for a fixed electron density defined by the Fermi energy  $\varepsilon_F = 10$  meV and two temperatures  $T_0 = \varepsilon_F$  and  $T_0 = 3\varepsilon_F$ . The corresponding values of the chemical potential are  $\mu_0 \approx -5.7$  meV and  $\mu_0 \approx -86$  meV, respectively. The latter case corresponds to the Boltzmann

distribution of electrons. Thermalization of electrons starts to play a role at  $T_0 \sim \varepsilon_F$ . As blue and red curves in Fig. 4 show, both circular and linear photoconductivities are suppressed by thermalization at  $\omega\tau_{ee} \lesssim 1$ , and this suppression becomes stronger with increase of temperature. However, such a suppression is not a general behavior. Thermalization aims to redistribute electrons over energy and it may cause either suppression or enhancement of the photoconductivity depending on how electron velocity and relaxation time  $\tau_1$  depend on energy. For instance, in the case of parabolic dispersion and Coulomb scatterers shown in Fig. 2, the thermalization does not affect  $\sigma_{xy}$  at all, because in that case  $H$  given by Eq. (25) is independent of energy.

## VI. SUMMARY

To summarize, we have studied the transverse photoconductivity of the 2DEG caused by intraband absorption of circularly and linearly polarized radiation. The transverse dc current has two contributions: (i) due to the optical alignment of electron momenta and (ii) due to the dynamic heating and cooling of the 2DEG. The heating contribution is dominant at low frequencies  $\omega\tau_0 \lesssim 1$ , where  $\tau_0$  is the energy relaxation time. In this range, the transverse photoconductivity reaches  $\sim 1\%$  of the dark conductivity of the 2DEG at  $1 \text{ W cm}^{-2}$  of the radiation intensity. At higher frequencies, the transverse current is determined by the relaxation of the first and second angular harmonics of the distribution function. We have developed the microscopic theory of transverse photoconductivity for arbitrary electron spectrum and scattering mechanisms. The value and the sign of the calculated photoconductivity of the 2DEG with parabolic and linear energy dispersion significantly depend on the scattering mechanism. Further, we have shown that thermalization processes caused by electron-electron collisions have a negligible impact on transverse photoconductivity of a nearly degenerate 2DEG, but may contribute considerably at higher temperatures, when the Boltzmann distribution is formed.

## ACKNOWLEDGMENTS

The author thanks S. A. Tarasenko and M. M. Glazov for fruitful discussions. The work was financially supported by the Basis Foundation for the Advancement of Theoretical Physics and Mathematics and RFBR Project No. 20-32-70048.

- [1] M. M. Glazov and S. D. Ganichev, High frequency electric field induced nonlinear effects in graphene, *Phys. Rep.* **535**, 101 (2014).
- [2] F. H. L. Koppens, T. Mueller, P. Avouris, A. C. Ferrari, M. S. Vitiello, and M. Polini, Photodetectors based on graphene, other two-dimensional materials and hybrid systems, *Nat. Nanotechnol.* **9**, 780 (2014).
- [3] X. Xu, N. M. Gabor, J. S. Alden, A. M. van der Zande, and P. L. McEuen, Photo-thermoelectric effect at a graphene interface junction, *Nano Lett.* **10**, 562 (2010).

- [4] X. Cai, A. B. Sushkov, R. J. Suess, M. M. Jadidi, G. S. Jenkins, L. O. Nyakiti, R. L. Myers-Ward, Sh. Li, J. Yan, D. K. Gaskill, T. E. Murphy, H. D. Drew, and M. S. Fuhrer, Sensitive room-temperature terahertz detection via the photothermoelectric effect in graphene, *Nat. Nanotechnol.* **9**, 814 (2014).
- [5] S. Castilla, B. Terrés, M. Autore, L. Viti, J. Li, A. Y. Nikitin, I. Vangelidis, K. Watanabe, T. Taniguchi, E. Lidorikis, M. S. Vitiello, R. Hillenbrand, K.-J. Tielrooij, and F. H. L. Koppens, Fast and sensitive terahertz detection using an

- antenna-integrated graphene p-n junction, *Nano Lett.* **19**, 2765 (2019).
- [6] M. Freitag, T. Low, F. Xia, and P. Avouris, Photoconductivity of biased graphene, *Nat. Photonics* **7**, 53 (2013).
- [7] L. Vicarelli, M. S. Vitiello, D. Coquillat, A. Lombardo, A. C. Ferrari, W. Knap, M. Polini, V. Pellegrini, and A. Tredicucci, Graphene field-effect transistors as room-temperature terahertz detectors, *Nat. Mater.* **11**, 865 (2012).
- [8] A. V. Muraviev, S. L. Rumyantsev, G. Liu, A. A. Balandin, W. Knap, and M. S. Shur, Plasmonic and bolometric terahertz detection by graphene field-effect transistor, *Appl. Phys. Lett.* **103**, 181114 (2013).
- [9] D. A. Bandurin, D. Svintsov, I. Gayduchenko, Sh. G. Xu, A. Principi, M. Moskotin, I. Tretyakov, D. Yagodkin, S. Zhukov, T. Taniguchi, K. Watanabe, I. V. Grigorieva, M. Polini, G. N. Goltsman, A. K. Geim, and G. Fedorov, Resonant terahertz detection using graphene plasmons, *Nat. Commun.* **9**, 5392 (2018).
- [10] J. Karch, P. Olbrich, M. Schmalzbauer, C. Zoth, C. Brinsteiner, M. Fehrenbacher, U. Wurstbauer, M. M. Glazov, S. A. Tarasenko, E. L. Ivchenko, D. Weiss, J. Eroms, R. Yakimova, S. Lara-Avila, S. Kubatkin, and S. D. Ganichev, Dynamic Hall Effect Driven by Circularly Polarized Light in a Graphene Layer, *Phys. Rev. Lett.* **105**, 227402 (2010).
- [11] M. V. Entin, L. I. Magarill, and D. L. Shepelyansky, Theory of resonant photon drag in monolayer graphene, *Phys. Rev. B* **81**, 165441 (2010).
- [12] P. A. Obraztsov, N. Kanda, K. Konishi, M. Kuwata-Gonokami, S. V. Garnov, A. N. Obraztsov, and Y. P. Svirko, Photon-drag induced terahertz emission from graphene, *Phys. Rev. B* **90**, 241416(R) (2014).
- [13] S. A. Tarasenko, Direct current driven by ac electric field in quantum wells, *Phys. Rev. B* **83**, 035313 (2011).
- [14] C. Drexler, S. A. Tarasenko, P. Olbrich, J. Karch, M. Hirmer, F. Müller, M. Gmitra, J. Fabian, R. Yakimova, S. Lara-Avila, S. Kubatkin, M. Wang, R. Vajtai, P. M. Ajayan, J. Kono, and S. D. Ganichev, Magnetic quantum ratchet effect in graphene, *Nat. Nanotech.* **8**, 104 (2013).
- [15] N. Kheirabadi, E. McCann, and V. I. Fal'ko, Cyclotron resonance of the magnetic ratchet effect and second harmonic generation in bilayer graphene, *Phys. Rev. B* **97**, 075415 (2018).
- [16] D. V. Fateev, K. V. Mashinsky, and V. V. Popov, Terahertz plasmonic rectification in a spatially periodic graphene, *Appl. Phys. Lett.* **110**, 061106 (2017).
- [17] Y. B. Lyanda-Geller, S. Li, and A. V. Andreev, Polarization-dependent photocurrents in polar stack of van der Waals solids, *Phys. Rev. B* **92**, 241406(R) (2015).
- [18] J. Quereda, T. S. Ghiasi, J.-S. You, J. van den Brink, B. J. van Wees, and C. H. van der Wal, Symmetry regimes for circular photocurrents in monolayer MoSe<sub>2</sub>, *Nat. Commun.* **9**, 3346 (2018).
- [19] Q. Ma, C. H. Lui, J. C. W. Song, Y. Lin, J. F. Kong, Y. Cao, T. H. Dinh, N. L. Nair, W. Fang, K. Watanabe, T. Taniguchi, S.-Y. Xu, J. Kong, T. Palacios, N. Gedik, N. M. Gabor, and P. Jarillo-Herrero, Giant intrinsic photoresponse in pristine graphene, *Nat. Nanotech.* **14**, 145 (2019).
- [20] J. Karch, C. Drexler, P. Olbrich, M. Fehrenbacher, M. Hirmer, M. M. Glazov, S. A. Tarasenko, E. L. Ivchenko, B. Birkner, J. Eroms, D. Weiss, R. Yakimova, S. Lara-Avila, S. Kubatkin, M. Ostler, T. Seyller and S. D. Ganichev, Terahertz Radiation Driven Chiral Edge Currents in Graphene, *Phys. Rev. Lett.* **107**, 276601 (2011).
- [21] S. Candussio, M. V. Durnev, S. A. Tarasenko, J. Yin, J. Keil, Y. Yang, S.-K. Son, A. Mishchenko, H. Plank, V. V. Bel'kov, S. Slizovskiy, V. Fal'ko, and S. D. Ganichev, Edge photocurrent driven by terahertz electric field in bilayer graphene, *Phys. Rev. B* **102**, 045406 (2020).
- [22] M. V. Durnev and S. A. Tarasenko, Edge photogalvanic effect caused by optical alignment of carrier momenta in two-dimensional Dirac materials, *Phys. Rev. B* **103**, 165411 (2021).
- [23] T. Oka and H. Aoki, Photovoltaic Hall effect in graphene, *Phys. Rev. B* **79**, 081406(R) (2009).
- [24] Yu. S. Gal'pern and Sh. M. Kogan, Anisotropic photoelectric effects, Soviet Physics JETP **29**, 196 (1969) [*Zh. Eksp. Teor. Fiz.* **56**, 355 (1969)].
- [25] V. I. Belinicher and V. N. Novikov, Non-equilibrium photoconductivity and influence of external fields on the surface photogalvanic effect, Sov. Phys. Semicond. **15**, 1138 (1981) [*Fiz. Tekh. Poluprovodn.* **15**, 1957 (1981)].
- [26] M. I. Karaman, V. P. Mushinskii, and G. M. Shmelev, Determination of the transverse photo-emf depending on the excited light polarization, Sov. Phys. Tech. Phys. **28**, 730 (1983) [*Zh. Tekh. Fiz.* **53**, 1198 (1983)].
- [27] S. K. Esayan, E. L. Ivchenko, V. V. Lemanov, and A. Yu. Maksimov, Anisotropic photoconductivity in ferroelectrics, Soviet Physics JETP Lett. **40**, 1290 (1984) [*Pis'ma Zh. Eksp. Teor. Fiz.* **40**, 462 (1984)].
- [28] D. V. Zavyalov, S. V. Kryuchkov, and T. A. Tyul'kina, Effect of rectification of current induced by an electromagnetic wave in graphene: A numerical simulation, *Semiconductors* **44**, 879 (2010) [*Fiz. Tekh. Poluprovodn.* **44**, 910 (2010)].
- [29] M. Trushin and J. Schliemann, Anisotropic photoconductivity in graphene, *Europhys. Lett.* **96**, 37006 (2011).
- [30] S. A. Sato, J. W. McIver, M. Nuske, P. Tang, G. Jotzu, B. Schulte, H. Hübener, U. De Giovannini, L. Mathey, M. A. Sentef, A. Cavalleri, and A. Rubio, Microscopic theory for the light-induced anomalous Hall effect in graphene, *Phys. Rev. B* **99**, 214302 (2019).
- [31] J. Ahn, G.-Yu. Guo, N. Nagaosa, and A. Vishwanath, Riemannian geometry of resonant optical responses, *arXiv:2103.01241*.
- [32] P. X. Nguyen and W.-K. Tse, Photoinduced anomalous Hall effect in two-dimensional transition metal dichalcogenides, *Phys. Rev. B* **103**, 125420 (2021).
- [33] C. M. Yin, N. Tang, S. Zhang, J. X. Duan, F. J. Xu, J. Song, F. H. Mei, X. Q. Wang, B. Shen, Y. H. Chen, J. L. Yu, and H. Ma, Observation of the photoinduced anomalous Hall effect in GaN-based heterostructures, *Appl. Phys. Lett.* **98**, 122104 (2011).
- [34] P. Seifert, F. Sigger, J. Kiemle, K. Watanabe, T. Taniguchi, C. Kastl, U. Wurstbauer, and A. Holleitner, In-plane anisotropy of the photon-helicity induced linear Hall effect in few-layer WTe<sub>2</sub>, *Phys. Rev. B* **99**, 161403(R) (2019).
- [35] J. W. McIver, B. Schulte, F.-U. Stein, T. Matsuyama, G. Jotzu, G. Meier, and A. Cavalleri, Light-induced anomalous Hall effect in graphene, *Nat. Phys.* **16**, 38 (2020).
- [36] S. Morina, O. V. Kibis, A. A. Pervishko, and I. A. Shelykh, Transport properties of a two-dimensional electron gas dressed by light, *Phys. Rev. B* **91**, 155312 (2015).

- [37] J. H. Strait, H. Wang, S. Shivaraman, V. Shields, M. Spencer, and F. Rana, Very slow cooling dynamics of photoexcited carriers in graphene observed by optical-pump terahertz-probe spectroscopy, *Nano Lett.* **11**, 4902 (2011).
- [38] J. C. W. Song, M. Y. Reizer, and L. S. Levitov, Disorder-Assisted Electron-Phonon Scattering and Cooling Pathways in Graphene, *Phys. Rev. Lett.* **109**, 106602 (2012).
- [39] V. I. Zemskii, B. P. Zakharchenya, and D. N. Mirlin, Polarization of hot photoluminescence in semiconductors of the GaAs type, *Pis'ma Zh. Eksp. Teor. Fiz.* **24**, 96 (1976).
- [40] V. D. Dymnikov, M. I. D'yakonov, and N. I. Perel, Anisotropy of momentum distribution of photoexcited electrons and polarization of hot luminescence in semiconductors, *JETP* **44**, 1252 (1976).
- [41] I. A. Merkulov, V. I. Perel, and M. E. Portnoi, Momentum alignment and spin orientation of photoexcited electrons in quantum wells, *Zh. Eksp. Teor. Fiz.* **99**, 1202 (1991).
- [42] R. R. Hartmann and M. E. Portnoi, *Optoelectronic Properties of Carbon-Based Nanostructures: Steering Electrons in Graphene by Electromagnetic Fields* (LAP Lambert Academic, Saarbrücken, 2011).
- [43] L. E. Golub, S. A. Tarasenko, M. V. Entin, and L. I. Magarill, Valley separation in graphene by polarized light, *Phys. Rev. B* **84**, 195408 (2011).